

This is the peer reviewed version of the following article:

Structural interpretation of the energetic performances of a pure silica LTA-type zeolite / Confalonieri, Giorgia; Ryzhikov, Andrey; Arletti, Rossella; Quartieri, Simona; Vezzalini, Giovanna; Isaac, Carole; Paillaud, Jean-Louis; Nouali, Habiba; Daou, T. Jean. - In: PHYSICAL CHEMISTRY CHEMICAL PHYSICS. - ISSN 1463-9076. - 22:9(2020), pp. 5178-5187. [10.1039/C9CP06760D]

Terms of use:

The terms and conditions for the reuse of this version of the manuscript are specified in the publishing policy. For all terms of use and more information see the publisher's website.

18/12/2025 11:09

ARTICLE

Structural interpretation of the energetic performances of Pure Silica LTA-type Zeolite

Giorgia Confalonieri,^a Andrey Ryzhikov,^{*b,c} Rossella Arletti,^{*a} Simona Quartieri,^d Giovanna Vezzalini,^a Carole Isaac,^{b,c} Jean-Louis Paillaud,^{b,c} Habiba Nouali^{b,c} and T. Jean Daou^{b,c}

Received 00th January 20xx,
Accepted 00th January 20xx

DOI: 10.1039/x0xx00000x

High pressure intrusion-extrusion process of different electrolyte aqueous solutions (NaCl and CaCl₂, 2M and 3M) in hydrophobic pure-silica LTA zeolite was investigated for energetic purposes by means of *in situ* X-ray powder diffraction, porosimeter tests, thermogravimetric analysis and NMR spectroscopy. In addition, porosimeter tests, thermogravimetric analysis and NMR spectroscopy were performed. The intrusion pressure of the saline solutions was proved to be higher than that of pure water, with the highest value measured for CaCl₂, thus increasing the energetic performances of the system. The intrusion of NaCl solutions was irreversible (bumper behavior), whereas that of CaCl₂ solutions is partially reversible (shock absorber behavior). The structural investigation allowed interpreting these results on the basis of the different intrusion mechanisms, in turn induced by the different nature of the cations present in the electrolyte solutions. When Si-LTA is intruded by NaCl solution, firstly H₂O molecules penetrate the pores, leading to a higher silanol defect formation followed by the solvated ions. With CaCl₂, instead, due to a higher solvation enthalpy of Ca²⁺, a higher pressure is required for intrusion, and both H₂O and ions penetrate simultaneously at the same pressure. The structural refinements demonstrate i) a different arrangement of the extraframework species in the two systems ii) the intrusion of the salt solutions occurs through a strong desolvation of the ions iii) the salt/H₂O ratios of the intruded species are higher than those of the starting electrolyte solutions.

1. Introduction

High-pressure intrusion of nonwetting liquids in porous solids can be exploited for mechanical energy absorption and storage purposes.¹⁻¹⁰ The energy of the applied pressure is converted into energy of the solid-liquid interface. The systems based on water or electrolyte aqueous solutions and hydrophobic porous solids (pure silica zeolites, grafted silicas, Metal-Organic Frameworks), named heterogeneous lyophobic systems (HLS), are strongly promising in terms of energetic applications.¹¹⁻¹⁷ Pure silica zeolites (zeosils), particularly the ones prepared in fluoride medium - which allows working with low pH and slow crystallization, so decreasing considerably the defect amount¹⁸ - are known to have strong hydrophobic character. Since 2001, they have been studied by the intrusion-extrusion of water and aqueous solutions for this kind of application.¹⁹ Depending on the zeosil structure (pore system *i.e.* cage or channel, pore dimensions, defectivity), the “zeosil/H₂O” systems are able to restore, dissipate or absorb the supplied mechanical energy accumulated during the compression step, behaving as springs, shock absorbers or bumpers, respectively.^{11,20,21} The intrusion of aqueous saline solutions with high concentrations instead of pure water, considerably increases the intrusion pressure,

thus improving the energetic performance.²²⁻²⁴ The relative increase ($P_{\text{solution}}/P_{\text{H}_2\text{O}}$) is particularly high for small pore zeosils (8 membered-rings (MR)).²⁵⁻²⁷ For example, the highest relative increase (by 7.4 times) was obtained for the intrusion of LiCl saturated solution (20 M) in LTA-type zeosil (*i.e.* with 3D channel system and 8MR openings (diameter = 0.41 nm)).

The rise of intrusion pressure using aqueous saline solutions can be explained considering several parameters: (i) increase of liquid-solid interfacial tension,²⁸ (ii) confinement effects,²⁹ (iii) osmotic phenomena³⁰ and (iv) ion desolvation.³¹ The distortion of the solvation shell and the desolvation of the ions during the penetration into the micropores seem to be the major factors affecting the intrusion pressure. The desolvation phenomenon was demonstrated in our previous studies, where the deformation of the zeosil framework during high pressure (HP) intrusion of water or salt solutions was monitored by *in situ* X-ray powder diffraction (XRPD).³² This structural approach allows unraveling the arrangement of the intruded species inside the pores. In particular, it was shown that during the intrusion of MgCl₂ solution (MgCl₂ · 21 H₂O) in FER-type zeosil, the intruded species had a salt/H₂O ratio (MgCl₂ · 10 H₂O) close to that of the saturated solution.³² In the case of the intrusion of NaCl, NaBr and CaCl₂ solutions in pure silica chabazite, the effect was even more pronounced³³: the salt/H₂O ratio of the intruded species was considerably higher than that of the corresponding saturated salt solutions, with a decrease of the ratio by 3-10 times in comparison with the initial ones.³³ Noteworthy, it was also observed a change in the salt/H₂O ratio of the intruded species during *P* rising. Another peculiarity of the intrusion of highly concentrated salt solutions is the change of the intrusion-extrusion behaviour. Generally, the increase of salt concentration leads to an improvement of intrusion reversibility in the case of “zeosil/solution” systems, demonstrating a fully or partially irreversible intrusion

^a Dipartimento di Scienze Chimiche e Geologiche (DSCG), Università di Modena e Reggio Emilia, Italy

^b Université de Haute Alsace (UHA), Axe Matériaux à Porosité Contrôlée (MPC), Institut de Science des Matériaux de Mulhouse (IS2M), Mulhouse, France

^c Université de Strasbourg, Strasbourg, France

^d Dipartimento di Scienze Matematiche e Informatiche, Scienze Fisiche e Scienze della Terra, Università di Messina, Messina S. Agata, Italy
Electronic Supplementary Information (ESI) available: [details of any supplementary information available should be included here]. See DOI: 10.1039/x0xx00000x

(bumper behaviour).^{25,34} It was also shown that the behavior of some systems depend on the anion and cation nature.^{35,36} The structural approach to the study of the evolution of the zeosils under water or electrolyte solution intrusion can provide a better understanding of the penetration mechanisms at atomistic level. The understanding of the interactions among the species confined in the microporous pure silica solids is essential for both fundamental and technological studies, since similar systems can be used for various technological applications (e.g. water desalination, ions and molecules separation, heterogeneous catalysis, etc.). Since it is known that the behaviour and the energetic performance of "zeosil/H₂O" or "zeosil/aqueous solution" systems depends crucially on the zeosil structure, it is important to study its influence on the penetration of solvated ions and the interactions with the framework. In this work, we selected LTA framework type, (*P6m3m* space group), constituted by cubooctahedral cages (named sodalite or β cages) connected by double 4-membered rings to form the larger α -cage.³⁷ A number of structural studies under pressure investigated this zeolite in its aluminosilicate sodium form (Na-LTA) using both penetrating and non-penetrating media,³⁷⁻⁴⁰ while only one experiment is reported on a pure-silica LTA (ITQ-29), testing its compressibility in the non-penetrating medium silicone oil.⁴¹ In the latter, the framework undergoes two phase transitions: one reversible at 1.2 GPa, and an order-to-order reconstructive one, at 3.2 GPa, with the transformation from ITQ-29 to ITQ-50. In the following, we will present the results of the HP intrusion-extrusion of NaCl and CaCl₂ aqueous solutions into a pure silica LTA-type zeolite, investigated through a multitechnique approach based on *in situ* XRPD at high pressure, porosimeter tests, thermogravimetric analysis (TG) and NMR spectroscopy.

2. Experimental

2.1. Zeolite synthesis

Pure silica LTA-type zeosil (from now on labelled Si-LTA) was obtained in fluoride medium using N-methyljulolidinium hydroxide (MJuOH, 4-methyl-2,3,6,7-tetrahydro-1H,5H-pyrido[3.2.1-ij]quinolinium hydroxide) and tetramethylammonium hydroxide (TMAOH) as organic structure-directing agents, according to the procedure described in previous works.^{42,43} Nanocrystals of LTA-type zeolite with Si/Al ratio of ~1 obtained previously⁴⁴ were used as seeds (2% mol.). Tetraethoxysilane (TEOS, Aldrich, 98%) was used as silica source. The reaction gel had the following molar composition: 1 SiO₂ : 0.25 MJuOH : 0.25 TMAOH : 0.5 HF (40%, Normapur) : 5 H₂O : 0.02 LTA seeds. The gel, transferred into a PTFE-lined stainless-steel autoclave, was heated at 135 °C for 48 hours. After synthesis, the solid (LTA-type zeolite with Si/Al ratio close to 50) was washed with deionized water and dried in an oven at 70 °C overnight. Then it was used as seeds for a second synthesis step, in the same conditions as the previous one, in order to obtain LTA-type zeolite with extremely

low aluminum content (no aluminum detected, Si/Al >1000). After the synthesis, the solid was washed with deionized water, dried in the oven at 70 °C overnight and calcined in air at 700 °C for 12 hours in order to remove the organic template.

2.2. Porosimetric measurements and other characterizations

The intrusion–extrusion tests of H₂O and aqueous salt solutions in Si-LTA were performed at room temperature using a Micromeritics mercury porosimeter (Model Autopore IV) in the *P* range 0.1–350 MPa. The measurements were carried out on zeolite pellets previously degassed at 300 °C under vacuum. The cell containing zeosil pellet and electrolyte aqueous solution consists of a polypropylene cylinder of 2 mL capacity, sealed using a mobile piston. This cell is introduced in the glass cell of the porosimeter, which is filled with mercury. The volume variation is determined from the capacity measurement, which depends on the height of mercury in the capillary tube of the glass cell. The experimental intrusion–extrusion curve is obtained after subtraction of the curve corresponding to the compressibility of the medium. Three intrusion–extrusion cycles for each solution (with measurement time of 1.5 hour per cycle, 10 sec of equilibrium time for each point) were performed. The values of the intrusion (*P*_{int}) and extrusion (*P*_{ext}) pressures correspond to that of the half volume total variation. The pressure is expressed in MPa, and volume variation in mL per gram of anhydrous calcined zeolite. The experimental error is estimated to 1% on the pressure and on the volume. 2M and 3M aqueous solutions of NaCl and CaCl₂ were used for the intrusion–extrusion experiments, in order to study the influence of the cation nature. The concentrations were chosen to be sufficiently high in order to observe the influence of the salt on the intrusion, but quite below the saturated ones, in order to avoid the possible salt crystallization under pressure.

2.3. NMR Spectroscopy and Thermogravimetric Analysis

Si-LTA- zeosil sample was characterized before and after intrusion–extrusion experiments by ²⁹Si MAS and ¹H–²⁹Si CPMAS NMR spectroscopy. Spectra were recorded on a Bruker Avance II 300 MHz spectrometer, with a double-channel 7 mm Bruker MAS probe, the recording conditions are given in Table S1 in the Supporting Information. TG analyses were carried out on a TG/DSC Mettler Toledo STARE system apparatus, under air flow, with heating rate of 5 °C/min, from 30 to 800 °C.

2.4. In situ XRPD at HP : data collection and treatment

X-ray Powder Diffraction experiments were performed at SNBL1 (BM01) beamline, ESRF, Grenoble, France. The pattern of Si-LTA at ambient pressure was measured using a boron-silicate glass capillary, while *in situ* data was collected as a function of pressure using a modified Merrill-Basset Diamond Anvil Cell.⁴⁵ The pressure was calibrated using the ruby fluorescence method⁴⁶ on a nonlinear hydrostatic pressure scale (estimated error is 0.05 GPa⁴⁷). Four aqueous solutions were used as Pressure Penetrating Media (PTM):

Table 1. Maximum pressure (*P* in GPa) reached during the XRPD experiments and pressure values at which it was possible to perform the refinement of the cell parameters and of the structure.

	Max <i>P</i> reached	<i>P</i> Cell Parameter	<i>P</i> Structural Refinements		Max <i>P</i> reached	<i>P</i> Cell Parameter	<i>P</i> Structural Refinements
Si-LTA/NaCl 2M	1.19	0.11, 0.14 0.24, 0.40, 0.59, 0.84	0.11, 0.14 0.24, 0.40	Si-LTA/NaCl 3M	0.60	0.12, 0.14, 0.28	0.12, 0.14
Si-LTA/CaCl ₂ 2M	2.15	0.17, 0.37, 0.63, 1.03 <i>P</i> _{amb} rev.	0.17, 0.37, 0.63	Si-LTA/CaCl ₂ 3M	1.27	0.17, 0.37, 0.53, 0.71	0.17, 0.37, 0.53

NaCl (2M and 3M) and CaCl_2 (2M and 3M). After each pressure increase the pressure was monitored and equilibrated for 10 minutes. Data was collected in Debye Scherrer geometry, with a wavelength of 0.68202 Å and diffraction images were recorded by Pilatus IP detectors (pixel dimensions 172 x 172 μm), with a sample distance of 239 mm. Dioptas software⁴⁸ was employed for the integration and treatment of the collected XRPD data.

Table 1 reports the maximum pressure reached in the various experiments and the pressure values for which unit cell parameters or structural refinements were satisfactory. From now on, various systems will be denoted shortly with the labels "Si-LTA/Salt", while Si-LTA/ H_2O will denote the zeolite intruded by pure water.

2.5. Structure Refinements

Structural refinements were performed by means of Rietveld method using GSAS package⁴⁹ and EXPGUI interface.⁵⁰ Structural data obtained refining Si-LTA at ambient pressure (P_{amb}) (Table S2 and S3 in Supporting Information) was used as starting model for HP refinements. The original space group $Pm\bar{3}m$ was maintained in the pressure range investigated and no phase transition was observed. After pressure release, due to the low data quality - as a consequence of a possible partial amorphization - only the cell parameters of Si-LTA/ CaCl_2 2M system were obtained.

Profile fitting was performed between 2.6 and 40° 2θ angle. The background was modeled using a Chebyshev polynomial with 30 coefficients, while the peak profile was refined using a Thomson pseudo-Voigt function,⁵¹ setting the peak cut-off at 0.1% of the peak maximum. Soft constraints were applied to Si-O distances (1.60 Å), and to some extraframework-extraframework distances, and their weight was gradually decreased (up to 10) after the initial stages of refinement. Localization of the extraframework sites was performed by inspection of the Fourier difference map. Isotropic thermal parameters were constrained to be equal for the atoms belonging to the same chemical species (except for the oxygen atoms, that were divided in two groups, those belonging to the framework and those to the extraframework).

3. Results

3.1. Porosimetric measurements

The intrusion-extrusion curves (P-V diagrams) of Si-LTA/ H_2O , Si-LTA/NaCl (2 and 3M) and Si-LTA/ CaCl_2 systems (2 and 3M) are shown in Figure 1. The curves are shifted along the Y-axis for a better visibility. Only the first cycle is presented for Si-LTA/ H_2O and Si-LTA/NaCl systems since the intrusion in the first cycle is fully irreversible, thus no intrusion is observed in the 2nd and the 3rd ones. On the contrary, all the three intrusion-extrusion cycles are shown for Si-LTA/ CaCl_2 systems. The measurements were performed up to

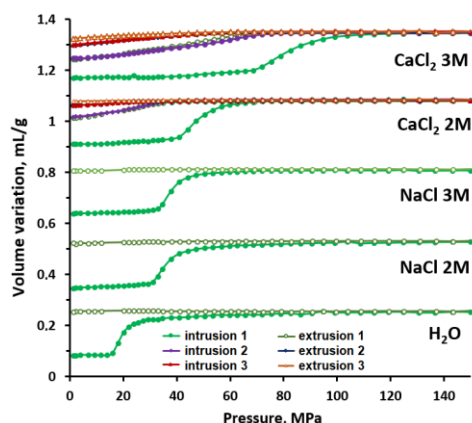


Figure 1. Intrusion-extrusion curves of Si-LTA/ H_2O , Si-LTA/NaCl 2M, Si-LTA/NaCl 3M, Si-LTA/ CaCl_2 2M and Si-LTA/ CaCl_2 3M systems. The curves are shifted along Y axis for better visibility.

the pressure of 350 MPa, but only the 0-150 MPa range is shown for better visibility, since no volume variation is observed at pressure higher than 110 MPa. The intrusion-extrusion characteristics are reported in Table 2.

In the first cycle, the intrusion is fully irreversible in the case of Si-LTA/ H_2O and both Si-LTA/NaCl 2M and 3M systems. These results on Si-LTA/ H_2O system are very close to the ones obtained in our previous work on the intrusion of water in LTA-type zeosil.²⁵ A partially irreversible intrusion is observed for Si-LTA/ CaCl_2 2M and 3M systems, demonstrating a combination of bumper (irreversible intrusion) and shock-absorber (reversible intrusion with relatively large hysteresis) behaviors. In the following cycles, the same behavior is observed, but the intruded volume decreases continuously, from 0.170 mL/g to 0.02 mL/g for Si-LTA/ CaCl_2 2M system and from 0.180 mL/g to 0.05 mL/g for Si-LTA/ CaCl_2 3M one for the 1st and 3rd cycle, respectively. Thus, a considerable difference is observed between the intrusion-extrusion behavior of Si-LTA/NaCl and Si-LTA/ CaCl_2 systems. It should be noticed that, in our previous work,²⁵ we observed a similar change of behaviour under intrusion of highly concentrated LiCl aqueous solutions in LTA-type zeosil, that was attributed to a strong difference of silanol defects formation between water and salt solutions. In order to verify this hypothesis,

Table 2. Characteristics of the Si-LTA/ H_2O and the Si-LTA/salt solution systems: intrusion (P_{int}) and extrusion (P_{ext}) pressures, intruded (V_{int}) and extruded (V_{ext}) volumes and energetic behavior.

System Si-LTA/	P_{int} (MPa)	P_{ext} (MPa)	V_{int} (mL/g)	V_{ext} (mL/g)	Behavior
H_2O	19	-	0.170	-	B
NaCl 2M	36	-	0.170	-	B
NaCl 3M	38	-	0.170	-	B
CaCl_2 2M	47*/20**	20*/14**	0.170*/0.06**	0.06*/0.02**/	B+SA*/B+SA**, ***
CaCl_2 3M	81*/47**	41*/26**	0.180*/0.10**	0.10*/0.05**/0.025***	B+SA*/B+SA**, ***

*First cycle. **Second cycles. ***Third cycles. B = Bumper, SA = Shock Absorber.

a characterization of the Si-LTA samples before and after intrusion-extrusion experiments was performed by thermogravimetric analysis and solid-state ^{29}Si NMR spectroscopy (see results below). The intrusion pressure increases with the salt concentration - from 19 MPa for H_2O up to 81 MPa for CaCl_2 3M aqueous solution. It is considerably higher for CaCl_2 solutions than for NaCl ones: 36 and 47 MPa for 2M solutions of NaCl and CaCl_2 , respectively, and 38 and 81 MPa for 3M ones. It should be also noticed that the increase of intrusion pressure with salt concentration (difference between P_{int} for 2M and 3M solutions) is much more pronounced in the case of CaCl_2 . These differences can be explained by a higher water solvation enthalpy and Gibbs energy of Ca^{2+} ions in comparison with Na^+ ones ($\Delta H = -1579$ kJ/mol and -406 kJ/mol⁵² and $\Delta G = -1505$ kJ/mol and -365 kJ/mol⁵³, respectively). These differences can be explained by a higher water solvation enthalpy of Ca^{2+} ions in comparison with Na^+ ones (-1579 kJ/mol and -406 kJ/mol, respectively, for the ions in gas phase^{52,53}). In order to penetrate inside the framework through small pore openings, the solvated ions should be partially desolvated. More energy is required to desolvate the ions with higher solvation enthalpy/Gibbs energy, thus, a higher pressure should be applied. Higher solvation energy corresponds to stronger interactions of H_2O molecules with the ions, not only in the first, but also in the second solvation shell. Thus, it is probable that more strongly bounded H_2O molecules in CaCl_2 solutions interact less with silanol defects, that can be another explanation of the higher reversibility of the intrusion of CaCl_2 solutions. The effect of lower interactions of the concentrated electrolyte solutions with silanol groups, leading to higher intrusion reversibility, has already been observed previously.²⁷ Another reason to explain the higher intrusion pressure could be the higher number of Cl⁻ ions in CaCl_2 solutions that should be desolvated compared to NaCl ones. Moreover, the different strength in ion pair interactions can also influence the intrusion pressure values.⁵⁴ In the case of CaCl_2 solutions, the decrease of the intrusion pressure from the 1st to the following cycles could be explained by the non-extruded ionic species and by the formation of hydrophilic silanol defects, which facilitate the next intrusions.

3.2. NMR Spectroscopy and TG analysis

These results are reported in detail in the Supporting Information and are briefly illustrated here. Before intrusion, Si-LTA sample presents very few defects, confirming its hydrophobic character. On the contrary, all the intruded samples have a considerable amount of silanol defects. Indeed, ^{29}Si MAS NMR spectra of Si-LTA samples after intrusion-extrusion performed by porosimetry, shown in Figures S1 and S2, exhibit the resonances corresponding to Q_3 groups ($\text{HO-Si}(\text{OSi})_3$ or $-\text{O-Si}(\text{OSi})_3$) at -98 ppm and Q_4 groups ($\text{Si}(\text{OSi})_4$) at -113 ppm, whereas only a well-defined resonance at -113 ppm is observed for non-intruded sample. The Q_3 sites represent about 12 % of the total silicon sites for the samples intruded with CaCl_2 solutions and 15 % in the case of H_2O and NaCl ones. ^1H - ^{29}Si CPMAS spectra (Figure S2) confirm such evolution of the signal of Q_3 groups. The results of the thermogravimetric analysis (Figure S3) are in good agreement with the ones of ^{29}Si NMR spectroscopy.

3.3. In situ HP XRPD

3.3.1 Unit Cell Parameter Evolution

Figure 2a and Table S4, reporting the cell volume evolution as a function of pressure, show that, up to 0.6 GPa, both Si-LTA/NaCl and Si-LTA/ CaCl_2 systems demonstrate a behavior similar to that of Si-

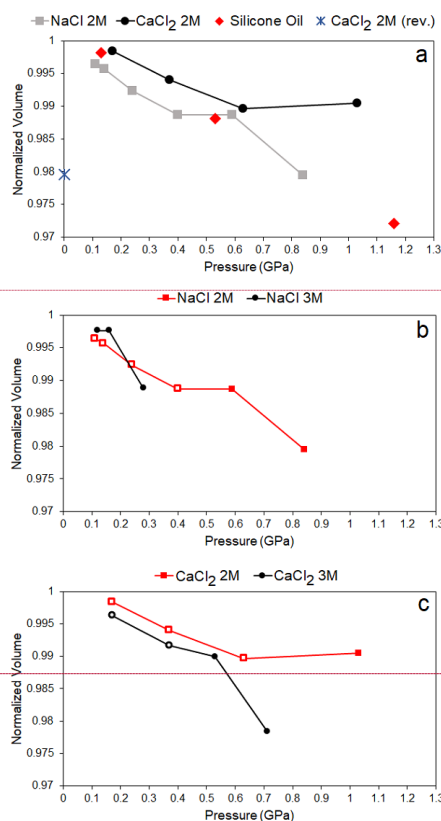


Figure 2. Normalized cell volume evolution as a function of P of Si-LTA intruded by a) NaCl 2M and CaCl_2 2M electrolyte aqueous solutions, plot also shows the data of the zeolite compressed in silicone oil.⁴¹ b) NaCl 2M and NaCl 3M, open symbols represent the experimental points at which the structure analysis was performed, while filled symbols represent the pressure values for which only the cell parameters were refined. c) CaCl_2 2M and CaCl_2 3M, open symbols represent the experimental points at which the structure analysis was performed, while filled symbols represent the pressure values for which only the cell parameters were refined. All values are normalized respect to the cell volume of Si-LTA at P_{amb} (collected in capillary). Error bars smaller than symbols

LTA compressed in silicone oil.⁴¹ The experiments performed at higher pressure on the two systems demonstrates that Si-LTA/NaCl 2M undergoes a further compression, while Si-LTA/ CaCl_2 2M system maintains almost the same cell volume. We cannot exclude that Si-LTA/ CaCl_2 2M could experiment an analogous volume decrease after the plateau, since the bad quality of the diffraction data prevent the determination of the cell volume above ~ 1 GPa.

To understand whether the compressibility is influenced by the solution concentration, a comparison between 2M and 3M concentrations of each electrolyte solution is reported in Figure 2b and 2c for Si-LTA/NaCl and Si-LTA/ CaCl_2 , respectively. No significant cell volume variations between 2M and 3M electrolyte solutions are

Commentato [RA1]: Giorgia referenza [53] Y. Marcus, *J. Chem. Soc., Faraday Trans.*, 1991, **87**, 2995-2999, <http://doi.org/10.1039/FT9918702995>

Commentato [RA2]: Giorgia referenza

Formattato: Evidenziato

Table 3. Number of Na⁺, Cl⁻ and H₂O molecules present in the unit cell of Si-LTA during intrusion of 2M and 3M NaCl solutions.

	Pressure (GPa)	W1	W2 and W2b	W3	W4	Na ⁺	Cl ⁻	Total H ₂ O
Capillary	P _{amb}	0.4				0	0	0.4
NaCl 2M	0.11		0.4			0	0	0.4
	0.14	1.4	2	0.1		0	0	3.6
	0.24		7.9	0.9		3	3	8.8
	0.40		7.7	0.7	0.3	3	3	8.7
NaCl 3M	0.12	1.7	1.6			0	0	3.3
	0.16	1.9	3.8			0	0	5.6

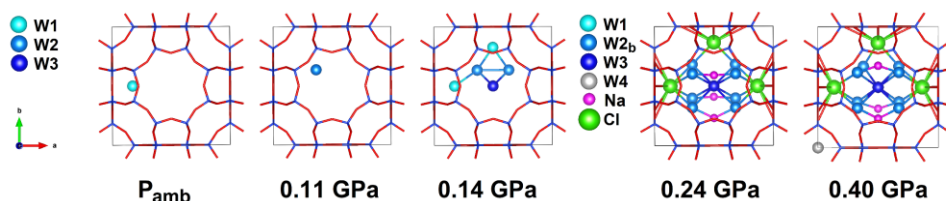


Figure 3. Evolution of the extra-framework sites as a function of pressure during the intrusion of NaCl 2M aqueous solution in Si-LTA. The figures show only the positions actually occupied, rather than all the partially occupied symmetrically equivalent positions.

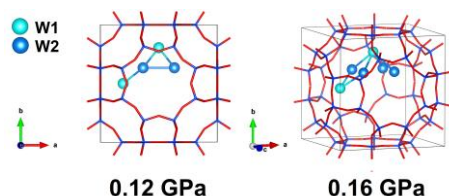


Figure 4. Evolution of the extra-framework sites as a function of the pressure during the intrusion of NaCl 3M aqueous solution in Si-LTA. The figures show only the positions actually occupied, rather than all the partially occupied symmetrically equivalent positions.

detectable from ambient pressure and 0.28 GPa and 0.53 GPa, for Si-LTA/NaCl and Si-LTA/CaCl₂, respectively. Instead, above 0.53 GPa the solution concentration markedly affects the compressibility of Si-LTA/CaCl₂ system.

As previously mentioned, the information on the reversibility of the *P*-induced cell volume modifications was obtained only for Si-LTA/CaCl₂ 2M, due to the partial amorphization of the other samples. For this system, the volume contraction is irreversible upon pressure release (Figure 2a).

3.3.2 . Extraframework contents of Si-LTA/NaCl 2M and 3M

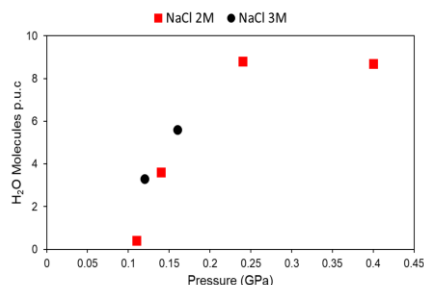
A structural description of the extraframework content of both 2M and 3M Si-LTA/salts systems is given in the related section of the Supplementary materials and from Table S5 to Table S9, also the observed and calculated profiles of the powder patterns, collected at the different pressure values, are showed as well (from Figure S4 to Figure S9).

Table 3, Figures 3 and 4 provide the structural information on the extraframework content determined for Si-LTA/NaCl 2M and 3M systems as a function of pressure.

Regardless the electrolyte concentration, both Si-LTA/NaCl systems experience the intrusion of only H₂O molecules between P_{amb} and

0.16 GPa (Table 3), arranged in a similar configuration (Figures 3 and 4). Figure 5 shows that the number of intruded H₂O molecules from 2M and 3M solutions follows the same trend as a function of pressure. This confirms that the starting step of the intrusion mechanism involves only H₂O molecules and seems to be independent on the solution concentration.

In Si-LTA/NaCl 2M, the ion intrusion occurs between 0.14 and 0.24

Figure 5. Pressure dependence of the H₂O content intruded into Si-LTA/NaCl 2M and 3M systems.

GPa (Figure 3). At 0.24 GPa, 9 H₂O molecules are present in the pores and are coordinated to the Na⁺ and Cl⁻ ions. Chloride anions are located at ~3.6–3.7 Å from eight framework oxygen atoms, that suggests the presence of O–H...Cl⁻ hydrogen bonds with the formed framework silanol groups (–Si–OH) pointing towards the chloride anions. The presence of silanol groups inside the intruded samples is confirmed by the results of both ²⁹Si MAS NMR spectroscopy and thermogravimetric analysis. At 0.40 GPa the extraframework species configuration is essentially maintained.

3.3.3 . Extraframework content of Si-LTA/CaCl₂ 2M and 3M

Table 4. Number of salt/H₂O molecules present in the unit cell of Si-LTA during the intrusion of 2M and 3M CaCl₂ solutions.

	Pressure (GPa)	W2	W3	W4b	Ca ²⁺	Cl ⁻	Total H ₂ O
CaCl ₂ 2M	0.17	2.4	0.6		0.8	1.7	3
	0.37	6.7	0.8		2.2	4.3	7.6
	0.63	6.5	0.8	0.4	2.3	4.6	7.7
CaCl ₂ 3M	0.17	2.4	0.1		0.8	1.7	2.5
	0.37	6.7	0.6		2.2	4.3	7.3

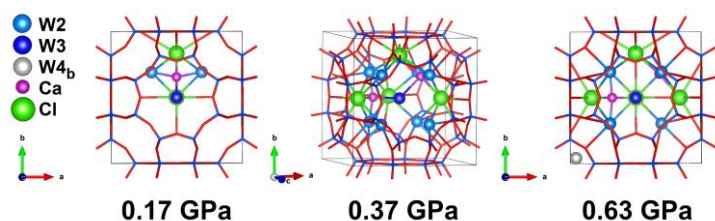
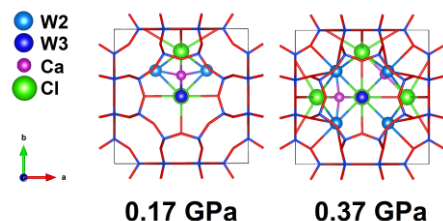
Figure 6. Structural evolution of the extra-framework sites as a function of P during the intrusion process of CaCl₂ 2M aqueous solution in Si-LTA. The figures show only the positions actually occupied rather than all the partially occupied symmetrically equivalent positions.Figure 7. Structural evolution of the extra-framework sites as a function of P during the intrusion process of CaCl₂ 3M aqueous solution in Si-LTA. The figures show only the positions actually occupied rather than all the partially occupied symmetrically equivalent positions.

Table 4 and Figures 6 and 7 show the extraframework content and distribution, as a function of pressure, in Si-LTA/CaCl₂ 2M and 3M systems.

Contrary to what observed for the NaCl solutions, during the intrusion of both 2M and 3M CaCl₂ solutions, both ions and H₂O molecules penetrate the LTA cage, already at 0.17 GPa. The structural data obtained for both concentrations are perfectly consistent up to 0.37 GPa. At 0.17 GPa, about 3 H₂O molecules, 0.8 Ca²⁺ cations and 1.7 Cl⁻ anions enter the zeolite pores (Table 4). Chloride and calcium ions are bonded each other and located in the main cage. The chloride anions interact with the framework oxygen atoms, again suggesting, as previously discussed, the presence of silanol defects on the zeolite framework. H₂O molecules are spread over two independent sites. Further details on the structures and the observed and calculated powder patterns are reported in the Supplementary Information (from Table S10 to Table S14 and from Figure S10 to Figure S14).

4. Discussion

In order to interpret the peculiar responses of the investigated systems, a multitechnique approach was used. Here, we will comparatively discuss the results obtained by the complementary techniques.

It must be underlined that in XRPD and porosimetric experiments different compression kinetics are induced and the pressure ranges cannot be compared directly. In fact, the two techniques explore different pressure ranges (GPa and MPa regimes for DAC and porosimeter, respectively), collecting a different number of data points in different time span. Specifically, due to the effect of the fast pressure increase occurring during the XRPD experiments, it is observable a lesser degree of pores filling, if compared to the filling observed at the same pressure in the porosimetric tests, where the increase of pressure is slower.

4.1. Influence of the electrolyte solution concentration

Figure 8 shows, for all the studied systems, the variation of the unit cell volume with P (Figure 8 a,b) compared with the variation of the available accessible volume (Figure 8 c,d), calculated starting from the accessible volume at ambient conditions (21.4 %) and subtracting the volume occupied by the intruded extraframework species.^{34,36}

In the investigated P range, the accessible volume decrease, derived by the penetration of extraframework species from the 2M and 3M solutions, is exactly the same in both Si-LTA/NaCl and Si-LTA/CaCl₂ systems, and this is reflected on similar cell volume. However, the sound interpretation of the influence of the electrolyte solution concentration on the intrusion is limited by the short pressure range in which it was possible to obtain reliable diffractometric data on the more concentrated systems (3M).

4.2. Influence of the nature and arrangement of extraframework species on the intrusion-extrusion process

The results of this work point to a considerable influence of the cation nature on the intrusion/extrusion process. The intrusion pressure measured by porosimeter is higher for Si-LTA/CaCl₂ in comparison to the Si-LTA/NaCl system. The initial compositions of the electrolyte solutions are CaCl₂/NaCl · 26 H₂O and CaCl₂/NaCl · 17 H₂O, for 2M and 3M concentrations, respectively. This implies that

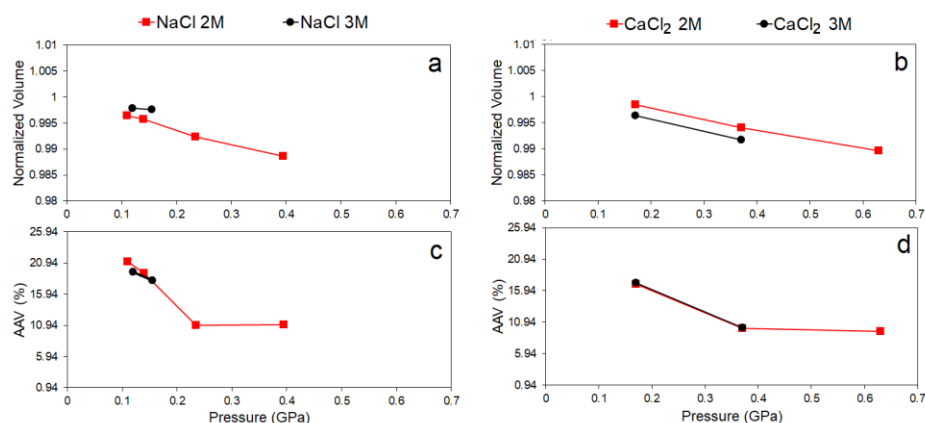


Figure 8. Evolution of unit cell volume and the available accessible volume (AAV) as a function of P in Si-LTA intruded by NaCl 2M and 3M (respectively a and c) and CaCl₂ 2M and 3M (respectively b and d) electrolyte aqueous solutions. The overall intruded volume was calculated considering the number of adsorbed species (H₂O molecules and ions) and their volume. Specifically, the adopted ionic and kinetics volumes are the following: $V_{\text{Na}^+} = 4.06 \text{ \AA}^3$, $V_{\text{Cl}^-} = 24.83 \text{ \AA}^3$, $V_{\text{Ca}^{2+}} = 4.19 \text{ \AA}^3$, $V_{\text{H}_2\text{O}} = 9.7 \text{ \AA}^3$.^{44,57} Error bars smaller than symbols

only a fraction of the H₂O molecules solvates the ions in their first solvation shell, while the others are involved in the second one. Due to a different water solvation enthalpy/Gibbs energy, H₂O molecules belonging to the first and the second solvation shells interact more strongly with Ca²⁺ ions than with Na⁺ ones. Therefore, hydrated Ca²⁺ cations require higher energy (*i.e.* intrusion pressure) to be desolvated and subsequently to penetrate inside the framework through the zeolite pore openings. XRPD results support this interpretation. In fact, when NaCl solutions are intruded, firstly, in the pressure range of 0.11–0.14 GPa, only H₂O molecules penetrate into the pores while the ions start to penetrate at higher pressure. In the case of CaCl₂ solutions, both ions and H₂O molecules are intruded into the zeolite pores simultaneously and at higher pressure (0.17 GPa). The penetration in two different steps of the NaCl solution components (H₂O and ions) may be due to the weaker interactions between ions and H₂O compared to CaCl₂ and to an higher ions/H₂O molecules ratio in CaCl₂ solutions. In fact, being the number of Cl⁻ ions higher in CaCl₂ solutions (concentrations 4M and 6M) the H₂O molecules are more bonded to the ions and thus tend to penetrate the pores along with them.

The second important aspect influenced by the cation nature is related to the bonding interactions of the intruded species inside the Si-LTA cage. Chloride anions occupy the same crystallographic position in both Si-LTA/CaCl₂ and Si-LTA/NaCl systems, forming Si-OH...Cl⁻ hydrogen bonds with the framework, although with different coordination number and distances (Table S6 and Table S11). The important point is that chloride ions interact differently with the cations in the two systems: in the case of Si-LTA/NaCl 2M both sodium and chloride are solvated by H₂O molecules and they are not directly bonded to each other. Otherwise, in Si-LTA/CaCl₂ 2M and 3M, Ca²⁺ and Cl⁻ ions are at a bonding distance of 2.8 Å, so forming "salt molecules". The differences in the extra-framework species arrangements and their bonding interactions at high pressure (Figure 3 and 6) can explain the different evolution of the

unit cell of the two investigated systems. Si-LTA is less compressible in the case of CaCl₂ aqueous solutions in comparison with NaCl one. The volume of intruded species is very close: Si-LTA/NaCl and Si-LTA/CaCl₂ exhibit a similar evolution of the pore filling (Figure 9) as a function of pressure, with a final stabilization at about 10–11%, corresponding to a filling of 55% of the overall accessible volume of Si-LTA (21.4%) (Figure 8c, 8d and 9). Considering the approximations in the accessible volume calculation, this result agrees with the data obtained by the porosimetric experiments, showing a maximum intruded volume corresponding to the filling of 65% of the overall accessible volume (0.17 mL/g) for both systems. This value is

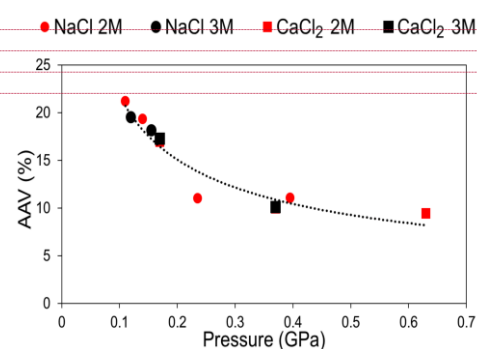


Figure 9. Available accessible volume as a function of P in Si-LTA intruded by NaCl and CaCl₂ 2M and 3M aqueous solution.

Formattato: Pedice

Formattato: Pedice

Formattato: Pedice

Formattato: Pedice

therefore the maximum filling that Si-LTA can experience in all the investigated systems. In this light, the lower compressibility of Si-LTA/CaCl₂ 2M in comparison to the Si-LTA/NaCl 2M can be interpreted as due to the peculiar extraframework species organization attained at HP. Moreover, this particular extraframework arrangement in Si-LTA/CaCl₂ 2M hinders the sample amorphization, which, instead, occurs in the other systems at HP.

The nature of the cation present in the intruded solution plays an important role also on the energetic behaviour of Si-LTA/solutions systems. The porosimetric data reveal that the intrusion process is irreversible or partially reversible for NaCl and CaCl₂ solutions, respectively. We can interpret this difference on the basis of structural results obtained at HP (0.40 GPa and 0.63 GPa for Si-LTA/NaCl and Si-LTA/CaCl₂, respectively), which are, however, available only for 2M solutions. In both systems Cl⁻ ions interact with the framework. However, the number of bonds and their lengths are different: in Si-LTA/NaCl chloride ions establish stronger interactions with the framework with respect to Si-LTA/CaCl₂ (8 bonds vs. 4). These stronger interactions likely prevent the extrusion of the extraframework species upon pressure release. The weaker framework-anion interactions in Si-LTA/CaCl₂ are probably due to the lower content of silanol defects formed under intrusion of CaCl₂ solutions in comparison to Si-LTA/NaCl systems, as shown by ²⁹Si MNR and TG experiments.

From our previous work ²⁵ it is known that intruded H₂O molecules induce the formation of silanol groups in Si-LTA framework. According to the present XRPD results on Si-LTA/NaCl systems, the solution intrusion occurs in two steps: firstly, H₂O molecules and then ions. On the contrary, in the case of CaCl₂ solutions, due to the high water solvation ~~enthalpy-energy~~ of Ca²⁺ ions, the ions are intruded together with H₂O molecules even at the beginning of the process. Thus, it can be supposed that: i) the first H₂O molecules intruded from the NaCl solutions are responsible for a higher formation of silanol groups on Si-LTA walls, and/or ii) the H₂O molecules more strongly involved in the ion solvation shells of the CaCl₂ solutions interact more weakly with Si-LTA framework. Both hypotheses can interpret the higher reversibility of the intrusion of Si-LTA/CaCl₂ system.

Table 5. Composition of the extraframework species determined at the highest investigated pressure after the intrusion of 2M NaCl and CaCl₂ solutions in Si-LTA and Si-CHA.

	P	NaCl 2M	P	CaCl ₂ 2M
	(GPa)		(GPa)	
Si-LTA	0.4	NaCl:2.9 H ₂ O	0.63	CaCl ₂ :3.4 H ₂ O
Si-CHA ³³	1.21	NaCl:3.6 H ₂ O	0.82	CaCl ₂ :5.8 H ₂ O

4.3. Comparison between Si-LTA and Si-CHA systems

In this section, we compare the results of our study on Si-LTA with those previously obtained by our groups on the intrusion of the same electrolyte solutions into pure-silica chabazite (Si-CHA), ³³ with the aim to understand the influence of the structure topology on the intrusion/extrusion process of electrolyte solutions in microporous materials.

For both zeolites, the use of electrolyte solutions instead of pure water induces a significant increase in the intrusion pressure, particularly in the case of the CaCl₂ solutions. Despite this, the kind and amount of the intruded species is different for the two zeolites (Table 5). Regardless pressure and salt composition, in Si-LTA/salt systems, a higher ions/H₂O ratio is observed into the porosities when compared to Si-CHA. Actually, this result could be interpreted on the basis of the amount of silanol defects. The initial Si-LTA used for the

study contains a smaller number of silanol defects with respect to Si-CHA, conferring a higher hydrophobic character to the framework, and disfavoring the H₂O molecules penetration.

Importantly, both Si-LTA and Si-CHA based systems are characterized by an ion/H₂O ratio (Table 5) higher than those of the corresponding initial electrolyte salt solutions, and even much higher than that of the corresponding saturated solutions. This confirms that the increase of the intrusion pressure achieved using electrolyte solutions instead of pure water is due to the desolvation of hydrated ions.

5. Conclusions

The intrusion of aqueous NaCl and CaCl₂ aqueous solutions in LTA-type zeosil has been studied by porosimetric experiments, high pressure *in situ* synchrotron XRPD, TG analysis and NMR spectroscopy, in order to better understand the mechanism of the process and the influence of electrolyte nature, zeolite topology and concentration of the electrolyte solutions.

We demonstrated that the salt/H₂O ratio of the intruded species (NaCl • 2.9 H₂O and CaCl₂:3.4 H₂O for NaCl and CaCl₂ solutions, respectively) is extremely higher than that of the initial solutions (CaCl₂/NaCl • 26 H₂O or CaCl₂/NaCl • 17 H₂O for 2M and 3M concentrations, respectively) and even higher than the one of the corresponding saturated electrolyte solutions (NaCl • 9H₂O and CaCl₂ • 6.6H₂O). Such compositions of the intruded species allow concluding that the intrusion of salt solutions occurs through the desolvation of hydrated ions.

The intrusion/extrusion process is strongly influenced by the cation nature. In the case of NaCl solutions, H₂O molecules are intruded firstly, followed by solvated ions at higher pressure. Otherwise, the intrusion of CaCl₂ solutions occurs *via* the penetration of the solvated ions. This can be related to the solvation ~~enthalpy-energy~~ of Ca²⁺ cation, that is much higher than that of Na⁺. This, in turn, can also explain the considerable increase of the intrusion pressure of CaCl₂ solutions in comparison with NaCl ones.

The intrusion of H₂O molecules and hydrated ions into the zeolite induces the formation of silanol defects, which mainly interact with the chloride anions. In the case of the intrusion of CaCl₂ solutions, the number of silanol defects as well as the strength of the framework-anion bonds are lower than in the case of NaCl ones. This explains the higher reversibility of CaCl₂ solution intrusion compared to Si-LTA/NaCl solution systems, which, instead, display a completely irreversible behavior.

Conflicts of interest

There are no conflicts to declare.

Acknowledgements

The authors thank the staff of SNBL1 (BM01) beamline at ESRF (Grenoble, France), for the assistance during XRPD data collection. Dr. Giorgia Confalonieri was supported by a grant awarded by the Italian Crystallography Association (AIC). This work was also supported by the Italian MIUR (PRIN2015 Prot. 2015HK93L7). The authors thank Université de Haute-Alsace and CNRS for providing facilities and funding as well as the characterization platforms of IS2M. Prof. T.J. Daou thanks IUF for financial support.

Notes and references

1. V. A. Eroshenko, *Int. Patent WO96/18040*, 1996.
2. V. A. Eroshenko, *URSS Patent 1333870*, 1985.
3. V. A. Eroshenko, A. Popyk *International Journal of Thermodynamics*, 2014, **17**, 33-41.
4. L. Coiffard, V. A. Eroshenko and J. P. E. Grolier, *AIChE*, 2005, **51**, 1246-1257.
5. A. Laouir, L. Luo, D. Tondeur, T. Cachot and P. Le Goff, *AIChE*, 2003, **49**, 764-781.
6. V. A. Eroshenko, I. Piatiletov, L. Coiffard and V. Stoudenets, *J. Proc. Mech. Eng., Part D: J. Automob. Eng.*, 2007, **221**, 301-312.
7. V. A. Eroshenko, *J. Proc. Mech. Eng., Part D: J. Automob. Eng.*, 2007, **221**, 285-300.
8. C. V. Suciu, T. Iwatsubo, K. Yaguchi and M. Ikenaga, *J. Coll. Inter. Sci.*, 2005, **283**, 196-214.
9. C. V. Suciu and K. Yaguchi, *Exp. Mec.*, 2009, **49**, 383-393.
10. V. A. Eroshenko, presented in part at the The Eight International Conference on Material Technologies and Modeling, MMT-2014, Ariel, Israel 2014.
11. L. Tzanis, M. Trzpit, M. Soulard and J. Patarin, *J. Phys. Chem. C*, 2012, **116**, 20389-20395.
12. V. A. Eroshenko and A. Y. Fadeev, *Colloid J.*, 1995, **57**, 446-449.
13. A. Y. Fadeev and V. A. Eroshenko, *J. Coll. Inter. Sci.*, 1997, **187**, 275-282.
14. T. Martin, B. Lefevre, D. Brunel, A. Galarneau, F. Di Renzo, F. Fajula, P. F. Gobin, J. F. Quinson and G. Vigier, *Chem. Commun.*, 2002, 24-25.
15. G. Ortiz, H. Nouali, C. Marichal, G. Chaplais and J. Patarin, *Phys. Chem. Chem. Phys.*, 2013, **15**, 4888-4891.
16. O. V. Ievtushenko, V. A. Eroshenko, Y. G. Grosu, J. M. Nedelec and J. P. E. Grolier, *Phys. Chem. Chem. Phys.*, 2013, **15**, 4451-4457.
17. G. Fraux, F. X. Coudert, A. Boutin and A. H. Fuchs, *Chem. Soc. Rev.*, 2017, **46**, 7421-7437.
18. M. A. Cambor, L. A. Villaescusa and M. J. Diaz-Cabanas, *Top. Catal.*, 1999, **9**, 59-76.
19. V. Eroshenko, R. C. Regis, M. Soulard and J. Patarin, *J. Am. Chem. Soc.*, 2001, **123**, 8129-8130.
20. L. Tzanis, M. Trzpit, M. Soulard and J. Patarin, *Microporous and Mesoporous Mater.*, 2011, **146**, 119-126.
21. A. Ryzhikov, I. Khay, H. Nouali, T. J. Daou and J. Patarin, *Rsc Advances*, 2014, **4**, 37655-37661.
22. L. Tzanis, H. Nouali, T. J. Daou, M. Soulard and J. Patarin, *Mater. Lett.*, 2014, **115**, 229-232.
23. A. Han and Y. Qiao, *J. Mater. Res.*, 2007, **22**, 644-648.
24. A. J. Han, W. Y. Lu, T. W. Kim, V. K. Punyamurtula and Y. Qiao, *Smart Materials & Structures*, 2009, **18**, 5.
25. A. Ryzhikov, L. Ronchi, H. Nouali, T. J. Daou, J. L. Paillaud and J. Patarin, *J. Phys. Chem. C*, 2015, **119**, 28319-28325.
26. L. Ronchi, A. Ryzhikov, H. Nouali, T. J. Daou and J. Patarin, *J. Phys. Chem. C*, 2018, **122**, 2726-2733.
27. L. Ronchi, A. Ryzhikov, H. Nouali, T. J. Daou and J. Patarin, *New J. Chem.*, 2017, **41**, 2586-2592.
28. E. W. Washburn, *Proc. Natl. Acad. Sci. U.S.A.*, 1921, **7**, 115-116.
29. A. J. Han, W. Y. Lu, T. Kim, X. Chen and Y. Qiao, *Phys. Rev. E*, 2008, **78**.
30. M. Michelin-Jamais, C. Picard, G. Vigier and E. Charlaix, *Phys. Rev. Lett.*, 2015, **115**.
31. M. Soulard, *France Patent FR2976030*, 2011.
32. R. Arletti, L. Ronchi, S. Quartieri, G. Vezzadini, A. Ryzhikov, H. Nouali, T. J. Daou and J. Patarin, *Microporous and Mesoporous Mater.*, 2016, **235**, 253-260.
33. G. Confalonieri, A. Ryzhikov, R. Arletti, H. Nouali, S. Quartieri, T. J. Daou and J. Patarin, *J. Phys. Chem. C*, 2018, **122**, 28001-28012.
34. A. Ryzhikov, I. Khay, H. Nouali, T. J. Daou and J. Patarin, *Phys. Chem. Chem. Phys.*, 2014, **16**, 17893-17899.
35. A. Ryzhikov, H. Nouali, T. J. Daou and J. Patarin, *Phys. Chem. Chem. Phys.*, 2018, **20**, 6462-6468.
36. A. Ryzhikov, H. Nouali, T. J. Daou and J. Patarin, presented at the IZC-2019, Perth, Australia, 2019.
37. A. Y. Likhacheva, M. E. Malyshev, A. Y. Manakov, S. V. Goryainov and A. I. Ancharov, *Z. Kristallogr.*, 2009, **224**, 137-143.
38. R. M. Hazen, *Science*, 1983, **219**, 1065-1067.
39. R. M. Hazen and L. W. Finger, *J. Appl. Phys.*, 1984, **56**, 1838-1840.
40. R. Arletti, O. Ferro, S. Quartieri, A. Sani, G. Tabacchi and G. Vezzadini, *Am. Mineral.*, 2003, **88**, 1416-1422.
41. J. L. Jorda, F. Rey, G. Sastre, S. Valencia, M. Palomino, A. Corma, A. Segura, D. Errandonea, R. Lacomba, F. J. Manjon, O. Gomis, A. K. Kleppe, A. P. Jephcoat, M. Amboage and J. A. Rodriguez-Velamazán, *Angew. Chem. Int. Ed.*, 2013, **52**, 10458-10462.
42. Y. Bouizi, J. L. Paillaud, L. Simon and V. Valtchev, *Chem. Mater.*, 2007, **19**, 652-654.
43. A. Corma, F. Rey, J. Rius, M. J. Sabater and S. Valencia, *Natur.*, 2004, **431**, 287-290.
44. S. Mintova, N. H. Olson, V. Valtchev and T. Bein, *Science*, 1999, **283**, 958-960.
45. R. Miletich, D. R. Allan and W. F. Kush, in *Rev. in Mineral. Geochem.* Mineralogical Society of America and Geochemical Society Washington, USA, 2000, vol. 41, pp. 445-519.
46. R. A. Forman, G. J. Piermarini, J. D. Barnett and S. Block, *Science*, 1972, **176**, 284-285.
47. K. H. Mao, J. Xu and P. M. Bell, *J. Geophys. Res.*, 1986, **91**, 4673.
48. C. Prescher and V. B. Prakapenka, *High Pressure Res.*, 2015, **35**, 223-230.
49. C. A. Larson and R. B. Von Dreele, *General Structure Analysis System "GSAS"*, Los Alamos, 1994.
50. B. H. Toby, *J. Appl. Crystallogr.*, 2001, **34**, 210-213.
51. P. Thompson, D. E. Cox and J. B. Hastings, *J. Appl. Crystallogr.*, 1987, **20**, 79-83.
52. D. W. Smith, *J. Chem. Educ.*, 1977, **54**, 540-542.
53. ~~Y. Marcus, *J. Chem. Soc., Faraday Trans.*, 1991, **87**, 2995-2999~~
54. ~~C. Held, L. F. Cameretti, G. Sadowski, *Fluid Phase Equilibria*, **270**, 2008, 87-96.~~
55. ~~C. Held, T. Reesche, S. Mohammad, A. Luza, G. Sadowski, *Chemical Engineering Research and Design*, **92**, 2014, 2884-2897.~~
5356. C. Baerlocher and L. B. McCusker, Database of Zeolite Structures. In <http://www.iza-structure.org/databases/>.
5457. S. K. Lilov, *Cryst. Res. Technol.* **1986**, **21**, 1299-1302.

Formattato: Tipo di carattere: Non Grassetto, Corsivo

Formattato: Tipo di carattere: Corsivo

Formattato: Tipo di carattere: Grassetto

Formattato: Tipo di carattere: Corsivo

Formattato: Tipo di carattere: Grassetto